Experiments in Fluids 37 (2004) 883–898
DOI 10.1007/s00348-004-0877-0

Surface selections and topological constraint evaluations for flow field analyses

John F. Foss

Abstract The isolated singular points (nodes, saddles) of a continuous vector field (e.g., velocity, shear stress, pressure gradient, vorticity, etc.) that are overlaid on a given surface must be compatible with the Euler characteristic of that surface, $X_{surface}$. All surfaces can be fashioned from a sphere plus handles plus holes, and $X_{surface}=2-\Sigma holes-2\Sigma handles=\Sigma nodes-\Sigma saddles$. This establishes an a priori constraint for the nodes and saddles that can be tested against the observed vector field to determine whether the experimental (or computational) observations are compatible with the known constraint. Numerous examples, including a clarification of, and a correction to, published results are given.

1 Introduction

Computed and experimentally observed velocity fields may involve numerous locations on a given surface, either one that is in close proximity to a physical surface or one interior to the flow field, where the velocity magnitude is zero and the direction is, therefore, undefined. A considerable body of literature related to these isolated singular points and their contribution to the analysis of such flow fields exists.

Perry and Chong (1987) categorize the singular points on the basis of phase-plane methods. (This reference will be identified as PC in the following discussion). The reader is referred to that presentation for their characterization of the various types of singular points. As noted below, a simpler representation will suffice for the present purpose. Specifically, the *stable nodes*, *node-focus*, *stable-foci*, *center*, *unstable-foci*, *star node*, and *unstable nodes* of that reference will be identified as *nodes* herein. This designation (i.e., an unmodified *node*) follows from the operational method of identification presented below. The term *saddle* is, however, used in common with PC (1987).

In addition to the representation of individual singular points and their stability, which has been the primary focus of PC (1987) and the majority of the related earlier communications, it is of considerable interest and utility to provide an a priori identification of the *topological rule* that must be satisfied by the collection of singular points on a given surface. More precisely, we will herein address the "isolated zeros of a tangent vector field on a smooth manifold," where the *manifold* represents the fluid dynamic surface of interest and *isolated* distinguishes the points of interest from a separation line or attachment line. These elements are considered in detail below. The topological rule that is the central issue of this communication is formally known as the Poincare-Hopf theorem. Bredon (1993) and Milnor (1997) are recommended references that provide the formal bases for the description provided herein.

Many authors, including Tobak and Peake (1982) and Ruderich and Fernholz (1986), who address such considerations, utilize the paper by Hunt et al. (1978) as their primary reference. That seminal paper will be referred to as HAPW (after the authors) in the following discussion. For convenience, the algorithm (to be developed) that allows an a priori specification of the relative number of nodes and saddles on a given surface in a flow field will be referred to as the *Rule* in the present communication.

HAPW (1978) provides guidance in the utilization of the Rule for flows over surface-mounted obstacles, inclusive of ones with a "passage between the obstruction and the host surface." The artifact of "an extension of the surface of interest" to create an artificial sphere is utilized in that reference. The region of interest is then considered to be a part of this composite surface. They also state the consequences of the Rule for other flow geometries.

The present exposition provides an alternative approach to that of HAPW (1978) for the identification of the constraints that are placed upon a collection of isolated singular points. It also provides an alternative strategy to identify the surface for which the analysis is to be applied.

The surfaces of interest may be entirely within the boundaries of a flow field, they may exist on a portion of

Received: 6 April 2004 / Accepted: 17 August 2004
Published online: 30 October 2004

J. F. Foss
Department of Mechanical Engineering,
Michigan State University, East Lansing,
Michigan 48824, USA
E-mail: foss@egr.msu.edu

The author's original experience with the motivating elements for this exposition were gained as an Alexander von Humboldt Fellow at the University of Karlsruhe. Professor W. Rodi served as the research host for this experience. Grateful appreciation is expressed to the AvH and Professor Rodi. MSU mathematics colleagues, Professors R. Miller and J. McCarthy, have provided substantial guidance and instruction for the topological elements presented herein. Useful discussions and clarifications were also gained from a 1995 interaction with Professors A.E. Perry and M.S. Chong at the University of Melbourne. Expert assistance with the preparation of the figures has been provided by M. Dusel and A. Butki.

the bounding physical surface, or they may totally reside on the bounding surface. In its most elementary form, the Rule states that a continuous vector field, overlaid on a sphere, will exhibit two nodes if the most simple pattern is present. This result is given the expression, "the hairy sphere theorem," as the representation of the simplest pattern into which the hairs (from root-to-tip as representatives of the vectors in the continuous vector field) can be smoothly arranged on the surface of the sphere. As emphasized in the following examples, the hairs may reside on either the exterior or interior of the sphere. Also, as will be evident below, a *sphere* means any surface that could be formed by the continuous deformation of either the inner or the outer surface of an inflated ball.

The Rule, to be described, applies equally to any vector field. Fluid mechanical examples include the (obvious) velocity field, which may involve its instantaneous, phase or conditionally averaged, or time-averaged representation. The streamlines in each of these fields are a useful technique to characterize their continuous nature. The vorticity field, as well as the associated vorticity filaments, provide a direct analogy to the velocity and the associated streamline fields. The pressure gradient can also be used as a whole-field variable of interest. The surface shear stress field is of particular importance in many experimental investigations and it bears a simple relationship to the velocity field for a linearly viscous fluid, as considered in detail below (Sect. 2.1).

As emphasized by HAPW (1978), given a body of experimental observations, it is often the case that some of the singular points are distinctly evident, whereas others are more difficult to discern from the available observations. Similarly, in a numerical simulation or an experiment, one portion of the flow may converge to a stable state sooner than another portion, and this behavior can lead to an incorrect assessment of the complete flow field.

It is the premise of this communication that a generalized procedure which can be confidently employed to assess the self-consistency of experimental or computational vector field results will be a useful addition to the literature on topological considerations in fluid dynamics. The identification of the separate surfaces and the application of the relevant expression of the Rule is particularly valuable in these cases.

Hence, the objective of the present communication is to provide, in the spirit of HAPW (1978), but with different mechanics, *a methodology that can be followed to establish the specific results of the Rule for a given surface in a given flow field*. As will be evident in this exposition, the identification of multiple surfaces in a given flow field is often required to confidently identify the separate singular points in that flow field.

The individual sections of this communication are to serve the stated objective. Section 2 identifies the attributes of the vector field that will serve as the bases of the present analysis. Section 3 presents the surfaces, and their topological identifications, upon which the subject vector field is established. Section 4 considers surface-mounted obstacles using the current formulation and that of HAPW (1978). Section 5 presents examples from the open literature, as well as examples that have been created for the present communication, which demonstrate the principles of Sects. 2 and 3. A summary is provided in Sect. 6.

2
The vector field and its singular points

2.1
Vector fields and the associated surfaces

For convenience, and because the number of applicable cases is large enough to warrant the restrictions, a single-phase Newtonian fluid will be considered for the present analysis of the velocity field. (The motivation for these restrictions will be evident in Eq. 1.) The subject vector fields are those that exist in the neighborhood of physical surfaces or that are projected onto a designated surface in the interior of a flow field. These two surfaces are referred to as *no slip* and *free slip*, respectively, by PC (1987), and this terminology is adopted herein. As noted in the examples below, a given surface may incorporate both attributes. The corresponding terms *body fitted* and *collapsed* are also descriptive of the surfaces that are compatible with the present methodology. These terms will be respectively used interchangeably with those of PC (1987).

As previously characterized by numerous authors, e.g., Lighthill (1963), HAPW (1978), and PC (1987), the subject vector field is defined by the following operations in the neighborhood of a physical surface. Here, n is the outward drawn normal from the physical surface, μ is the fluid viscosity, and $\vec{\tau}_w$ is the vector shear stress $\mu\frac{\partial\vec{V}}{\partial n}\Big]_{n=0}$ at the surface. These symbols are graphically represented in Fig. 1. Note that $\vec{\tau}_w \times \hat{s} = 0$ introduces $\hat{s}$ as the direction of the streamlines in the neighborhood of the surface. The vector field of interest is, then, the velocity at the small distance (δn) "above" the surface, as defined by:

$$\vec{V}(\delta n) = \left\{ \frac{\partial \vec{V}}{\partial n}\Big]_{n=0} \delta n \right\} \tag{1}$$

"Small distance" can be given substance by noting that $\left[\frac{(\delta n)u_\tau}{\nu}\right] \ll 1$ or

$$\delta n \ll \left[\frac{\nu}{(\partial V/\partial n)_{n=0}}\right]^{1/2} \tag{2}$$

where ν is the kinematic viscosity of the fluid.

Either the condition of an incompressible flow, Dρ/Dt=0, or a steady flow, $\partial\rho/\partial t = 0$, plus the no penetration condition at a solid surface (i.e., no suction or blowing) ensures that $\vec{V}(\delta n)$ is tangential to the adjacent surface, except in the neighborhood for which τ_w=0. Specifically, from:

$$\frac{\mathrm{D}\rho}{\mathrm{D}t} + \rho\nabla\cdot\vec{V} = 0$$

and for $\vec{V}(n=0) = 0$, the indicated constraints result in the condition $\nabla\cdot\vec{V} = 0$ at $n = 0$. Hence, the component of the velocity normal to the wall, $V_\mathrm{n}(\delta n)$, is second order in δn as:

$$V_\mathrm{n}(\delta n) = \underset{(=0)}{V_\mathrm{n}(0)} + \underset{(=0)}{\frac{\partial V_\mathrm{n}}{\partial n}\delta n} + \frac{\partial^2 V_\mathrm{n}}{\partial n^2}\Big]_0 \frac{\delta n^2}{2} + \ldots \tag{3}$$

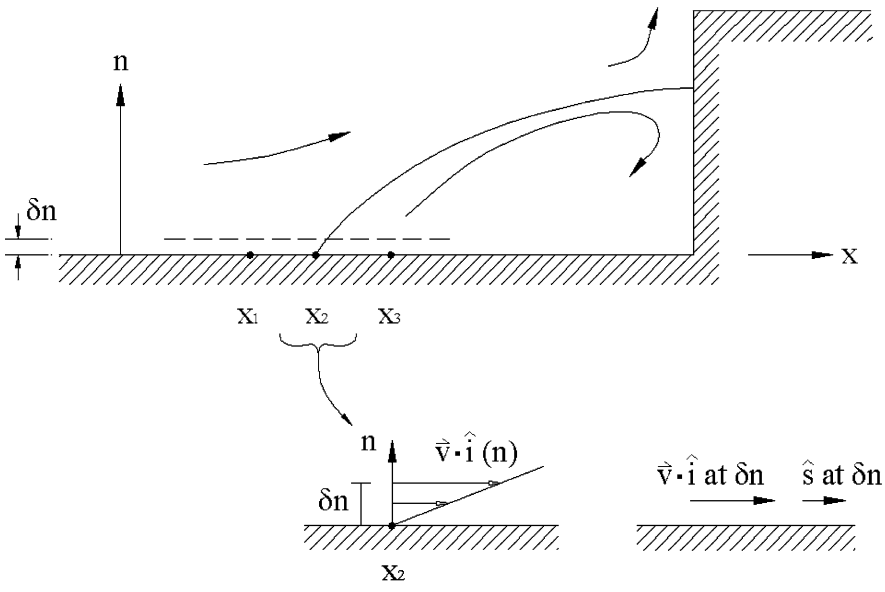

Fig. 1. Relationship of the wall shear stress ($\vec{\tau}_w$) to the subject velocity field $\vec{V}(\delta n)$

Since the velocity component tangential to the surface (V_s) is, in general, first order in δn, a singular point in the velocity field at δn will only occur above a location of zero shear stress where:

$$V_s(\delta n) = V_s(0) + \frac{\partial V_s}{\partial n}\delta n + \frac{\partial^2 V_s}{\partial n^2}\frac{\delta n^2}{2} + \ldots$$
$$= 0 + \left[\frac{\tau_w}{\mu}\right]\delta n + \left(\frac{\partial^2 V_s}{\partial n^2}\right)\frac{\delta n^2}{2 + \ldots} \quad (4)$$

Hence, as stated above, the subject velocity field $\vec{V}(\delta n)$, will exhibit a zero value above a location on a physical surface at which τ_w=0. This condition may exist at an isolated point (the subject of the present considerations) or as one point along a continuous curve that satisfies τ_w=0. The stagnation line on a torus that is oriented with its axis parallel to the approach flow is an example of the latter condition; see Fig. 2a. (The forward portion of the torus is of interest for this immediate example. If the axis of the torus is parallel to the approach flow, then the closed ring of stagnation points will exist. The aft portion of the flow will, for small and larger Reynolds numbers, separate in possibly complex patterns. If the aft region involves anything other than an axisymmetric flow pattern, the isolated nodes and saddles would have to be equal in number in order to satisfy the X=0 condition.) The condition that $\vec{V}(\delta n) = 0$ along a continuous curve has been identified as a *node-saddle* by PC (1987). See Fig. 5, case 1 of that reference for a graphical definition of a node-saddle.

The topological character of the flow field shown in Fig. 2a can be significantly altered by executing a "saw cut" through one portion of the (solid) torus; the altered geometry is shown in Fig. 2b. The upstream flow now

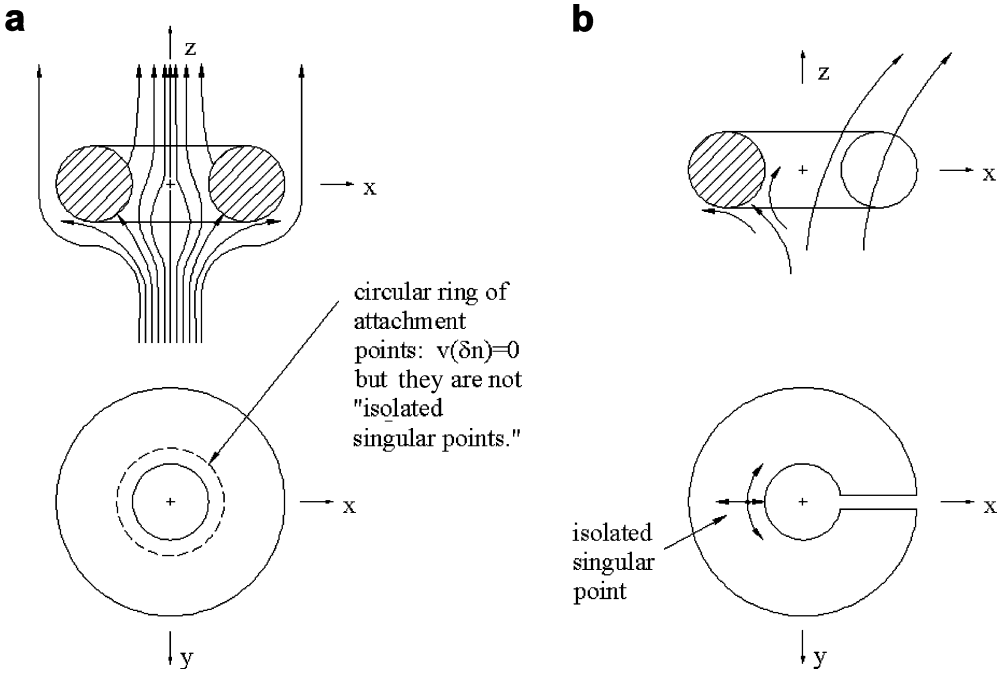

Fig. 2a, b. Two examples of surface identification and their relationship to a hydrodynamic flow field. **a** A torus with its axis parallel to the approach flow—a condition with no isolated singular points. **b** A sphere (created by the saw cut through the solid torus) with one attachment node shown. The balance of the singular points *must* yield one net node

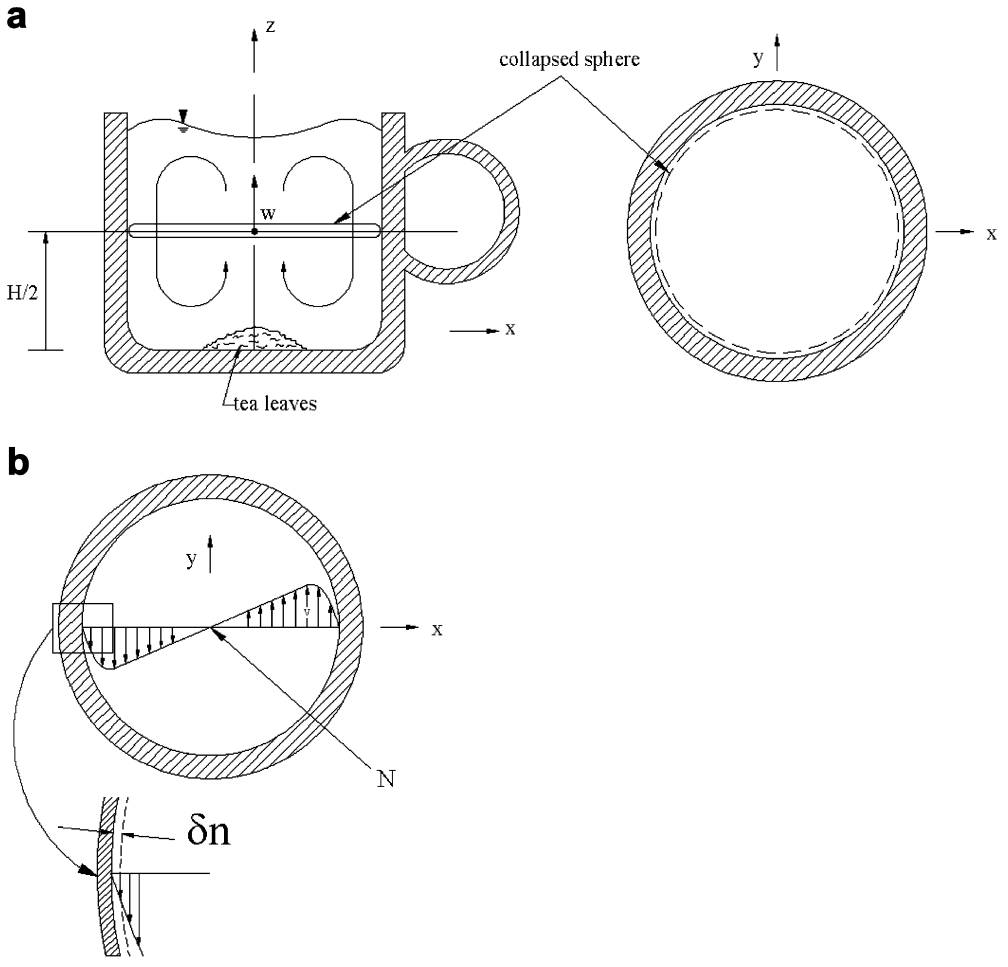

Fig. 3a, b. A stirred cup of liquid as an example of a singular point in a projected vector field. **a** The mid-height plane and the collapsed sphere. Note that the tea leaves indicate the presence of the secondary flow. **b** The velocity field in the plane of the collapsed sphere. The centered nodal points exist on the upper and the lower surfaces of the collapsed sphere

stagnates at one point instead of along a continuous and circular collection of "points." (Note that the finite size of a fluid dynamic particle disallows the substitution of the words "an infinity of points" for "collection of points" if one considers the fluid to be the substance that could be used in an experiment and not the "infinitely subdividable substance of the continuum approximation.") The three-dimensional flow near the saw cut can be expected to be rather complex. One can, however, be assured (Sect. 3.2) that the singular points will result in the addition of one net node to the node at the stagnation point for this newly constructed sphere. ("Net node" refers to the condition where K nodes and $K-1$ saddles may be added to the topology of the subject vector field. This is clarified in Sect. 3.)

Surfaces that are partially or completely in the interior of the flow will, as noted above, also be considered. In these cases, the relevant vector field is that which is projected onto the subject surface. In such a case, a singular point in the subject plane need not be characterized by $\vec{V} = 0$; it is only necessary that the projected $\vec{V}$ be zero. An instructive example is provided by a *stirred* cup, for which the subject plane is mid-way between the bottom of the cup and the free surface; see Fig. 3. The text following Eq. 7 clarifies the appropriate surface for this example. The secondary flow (as made evident by tea leaves or other solid material on the bottom of the cup) shows the presence of a radial inflow at this bottom surface with the concomitant vertically upward movement of fluid at the center of the "vortex." The resulting secondary flow is shown schematically in Fig. 3. Hence, $u=v=0$ (the projected velocity) at the central point in the subject plane albeit $\vec{V} = \hat{k}w$ is not zero at the same location.

2.2 Isolated singular points

An isolated singular point can be characterized by its Poincare index; the possible values are +1 and −1. The former characterizes a node; the latter describes a saddle. Additional information regarding Poincare indices can be found in Hurewicz (1958) and Davis (1962)[1]. The operational steps to identify the index for a candidate singular point also provide a useful "tool" for flow field analyses. These steps are shown in Fig. 4a, which makes use of the unstable focus as defined by PC (1987). The steps are described as:

1. Place a circle around the candidate singular point
2. Place the base of a unit vector on the circle in the direction of the local member of the vector field at that point
3. Cause the base of the unit vector to revolve, on the circle, clockwise around the candidate singular point

[1] These references were kindly supplied by a reviewer.

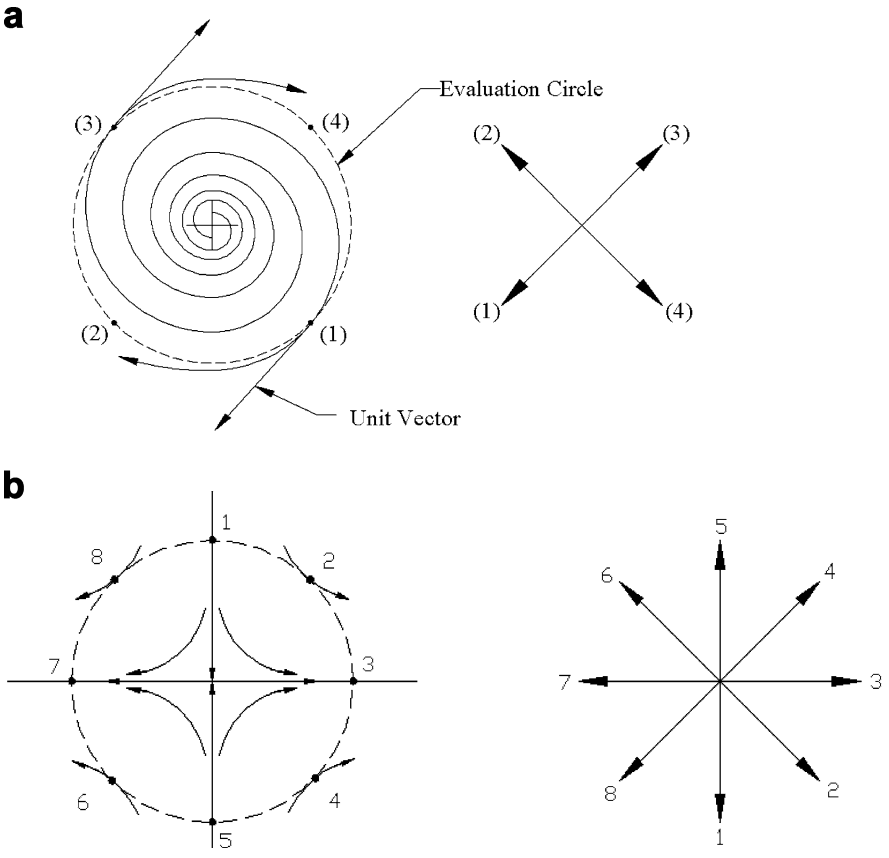

Fig. 4. a A representative node (unstable focus) and **b** a saddle

such that the vector is tangential to the local vector field at each point on the circumference of the circle
4. Following the above revolution, ascertain whether the unit vector has rotated 2π radians about its base during the translation of the vector's base around the circle

The following outcomes of this operation, and their interpretations, are (outcome; inference):

1. The vector has rotated 2π radians in the clockwise direction about its base point; a (net) node is enclosed within the circle
2. The vector has not rotated about its base point; there is no net singular point within the circle
3. The vector has rotated 2π radians in the counterclockwise direction about its base point; a (net) saddle is enclosed within the circle

It is apparent in Fig. 4a that the base has rotated 2π radians in the positive or clockwise direction. Hence, the enclosed singular point is a node. These operations, applied to the other foci and nodes of PC (1987) also yield an index of +1, which leads to the undifferentiated term, "node," in the present communication. If the same operations are performed for a "saddle," it is evident that the unit vector will rotate 2π radians in the counterclockwise direction; see Fig. 4b. This counterclockwise rotation identifies the enclosed singular point as a saddle with an index of −1.

Figure 5, taken from Perry and Chong (1994), provides a relevant example of the utility of this "tool" for flow field analyses. Specifically, the two interior circles reveal the presence of a node (upper left) and a saddle (lower right). No net rotation of the unit vector is observed as it revolves about the two inner circles on the path described by the encompassing circle.

3
Characteristics of surfaces

3.1
A sphere plus holes plus handles

Elementary considerations from topology show that any given surface can be formed by the addition of 0, 1,..., N handles on a sphere and/or "punching" 0, 1,..., M holes through its surface. (That is, an integer number of handles and holes.) It is important to recognize that the surface of interest may be formed from the interior or the exterior of the sphere and, of course, that the sphere is totally "malleable," which permits it to be deformed into any arbitrary shape that preserves the definition of a sphere[2].

Examples that will serve the interests of the later discussion are presented here to clarify the formation of such surfaces. These are designated as "six exemplar surfaces":

1. A sphere—an archer's arrow (Fig. 6) or the cut torus of Fig. 2b
2. A sphere plus one hole—an inlet valve of an IC engine (Fig. 7)
3. A sphere plus one handle—the torus of Fig. 2a

[2] A formal definition of a sphere is provided in the Appendix.

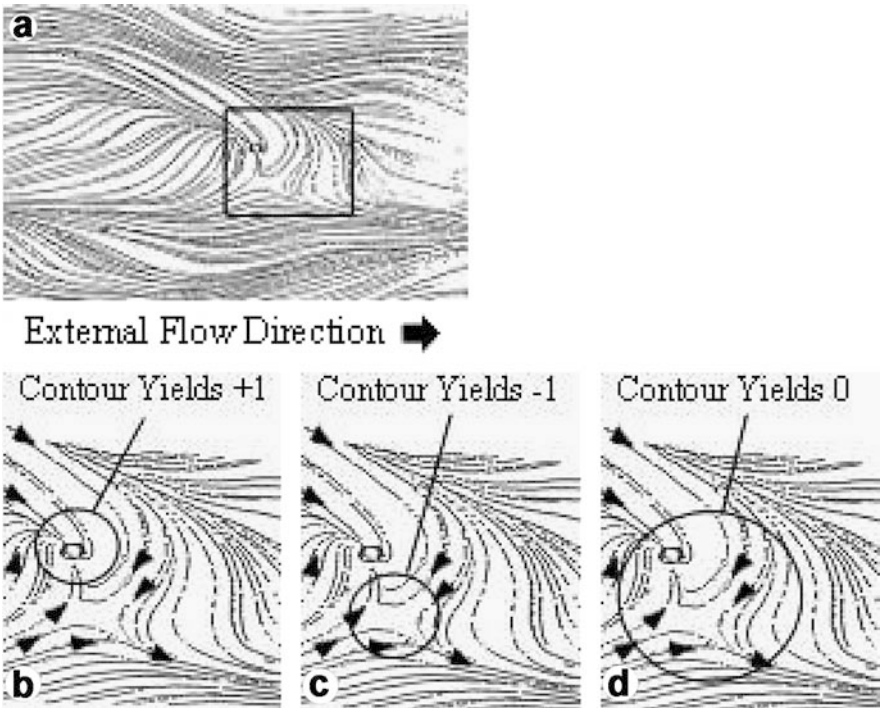

Fig. 5. Singular point identifications using the identification technique of Fig. 4

Fig. 6. An archer's arrow: a representative topological sphere

4. A sphere plus two holes—the flow past a surface-mounted obstruction (Fig. 11a)
5. A sphere plus three holes—the experiment of Ruderich and Fernholz (1986); see Fig. 8a
6. A sphere plus two holes plus one handle—a wind tunnel with a full-span model or the flow past a surface-mounted obstacle with a passageway (Fig. 11b). (Note that if the downstream surface of Fig. 8a were positioned downstream of the cross-member's trailing edge, then the correct surface would be a sphere plus two holes and a handle. This is the condition shown in Fig. 8b.)

An important constraint made explicit by Bredon (1993) and Milnor (1997) is that, *if a hole is present in the selected surface, then the vector field must either be directed uniformly inward—or outward—at the exposed edge.* This constraint will be clarified (Fig. 10) following the identification of the Euler characteristic and its relationship to the sum of the indices for a given surface.

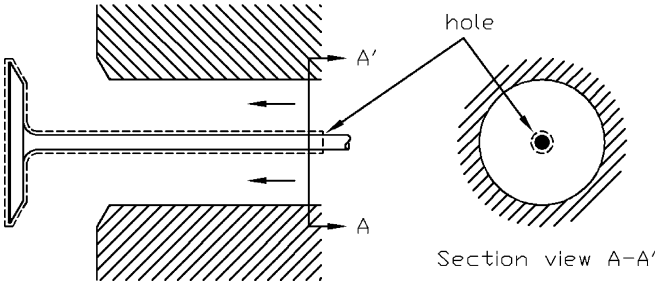

Fig. 7. The flow past an inlet valve of an IC engine: sphere plus one hole geometric surface

3.2
The Euler characteristic of a surface

The Euler characteristic (X) of a surface is a property that can be immediately inferred from the formation process. Specifically, the X value for a given surface is:

$$X_{\text{surface}} = X_{\text{sphere}} - 2\Sigma\text{handles} - \Sigma\text{holes} \qquad (5a)$$

which permits the X values of the above examples to be designated as shown in Table 1, given the condition that $X_{\text{sphere}}=2$. (The X_{sphere} value is clarified below).

The significance of the Euler characteristic for the present communication is its relationship to the Rule:

$$X_{\text{surface}} = \Sigma\begin{bmatrix}\text{indices of the vector field}\\ \text{singular points on the surface}\end{bmatrix} = \Sigma N - \Sigma S \qquad (6)$$

This relationship can be found in numerous sources, including Bredon (1993) and Milnor (1997). The X value for a sphere can be identified from Eq. 6 and the above noted hairy sphere theorem. It is considered to be apparent that the least complex arrangement of the hairs (the vector field) on a sphere (or, for clarity, a round ball) is to comb them from the "crown" to a "collection point" that is considered to exist at a distance of (for example) D (i.e., the sphere's diameter) from the crown. Both of these points represent a node (by application of the revolving vector test as clarified in Fig. 4). Hence, a sphere (no

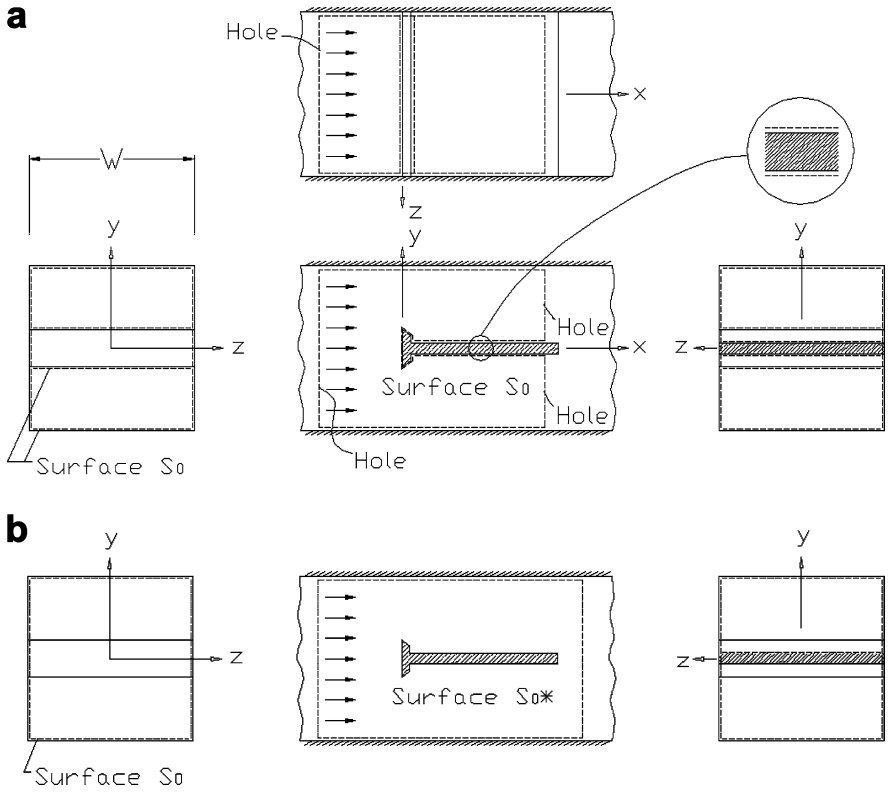

Fig. 8a, b. The experiment of Ruderich and Fernholz (1986) with two no-slip surfaces to represent their geometry. **a** A sphere plus three holes. **b** A sphere plus two holes plus one handle

handles, no holes in Eq. 5a) is characterized by two nodes (ΣN=2) and Eq. 5a can be rewritten as:

$$X_{\text{surface}} = 2 - 2\Sigma\text{handles} - \Sigma\text{holes} \tag{5b}$$

Note that Eq. 6 is also stated as Eq. 2.12 by HAPW (1978). However, as made evident below, the present communication utilizes this result in a manner that is somewhat different from that earlier communication.

HAPW introduce a most useful concept for the complete topological description of a flow field; specifically, they describe "... two-dimensional plane sections of the flow..." and state the appropriate form of the Rule for such surfaces. This concept can be set in the present context by noting that such a surface can be envisioned as the result of:

1. Starting with a sphere that touches the spanwise edges of a "planar" section of interest, and
2. Keeping these edges fixed as the sphere is "evacuated" and "collapses" to a "planar" surface with the desired boundaries at the lateral edges

The lateral edges, at which the velocity is required to be tangential to the boundary, will be referred to as *seams*. In keeping with a constraint stated above, an exposed edge (i.e., a hole for the collapsed surface) will involve only inward or only outward directed vectors with respect to the collapsed surface.

The collapsed sphere can be modified by the addition of handles and holes as above. The Rule does not, in principle, change with these additions; however, it is necessary to recognize that any singular point on a seam will appear once on the collapsed surface, whereas singular points interior to the seams will appear on two surfaces and must, therefore, be counted twice. Following HAPW (1978), the designation 1/2 nodes (N') and 1/2 saddles (S') describe the singular points on the seams whereas full nodes (N) and saddles (S) appear in the interior of the collapsed surface. Hence, Eq. 6 for a collapsed sphere is given the form noted in Eq. 7, namely:

$$X_{\text{surface}} = 2\Sigma N + \Sigma N' - 2\Sigma S - \Sigma S' \tag{7}$$

The mid-height (H/2) location of the stirred cup, Fig. 3, provides an immediate example. The selected surface is a collapsed sphere that forms a disc of negligible thickness and a diameter of $D-2\delta$n, where D is the diameter of the cup and δn of Fig. 3, like δn of Fig. 1, is a small distance into the flow. This small displacement allows the vector field that covers the surface (i.e., the vector velocity that is projected onto the surface) to be uniformly identified as the velocity components in the x–y plane. The velocity at

Table 1 X values for the exemplar surfaces

Example number	1	2	3	4	5	6
Figure number of the example surface	6, 2b	7	2a	11a	8a	8b, 11b
X_{surface}	+2	+1	0	0	−1	−2

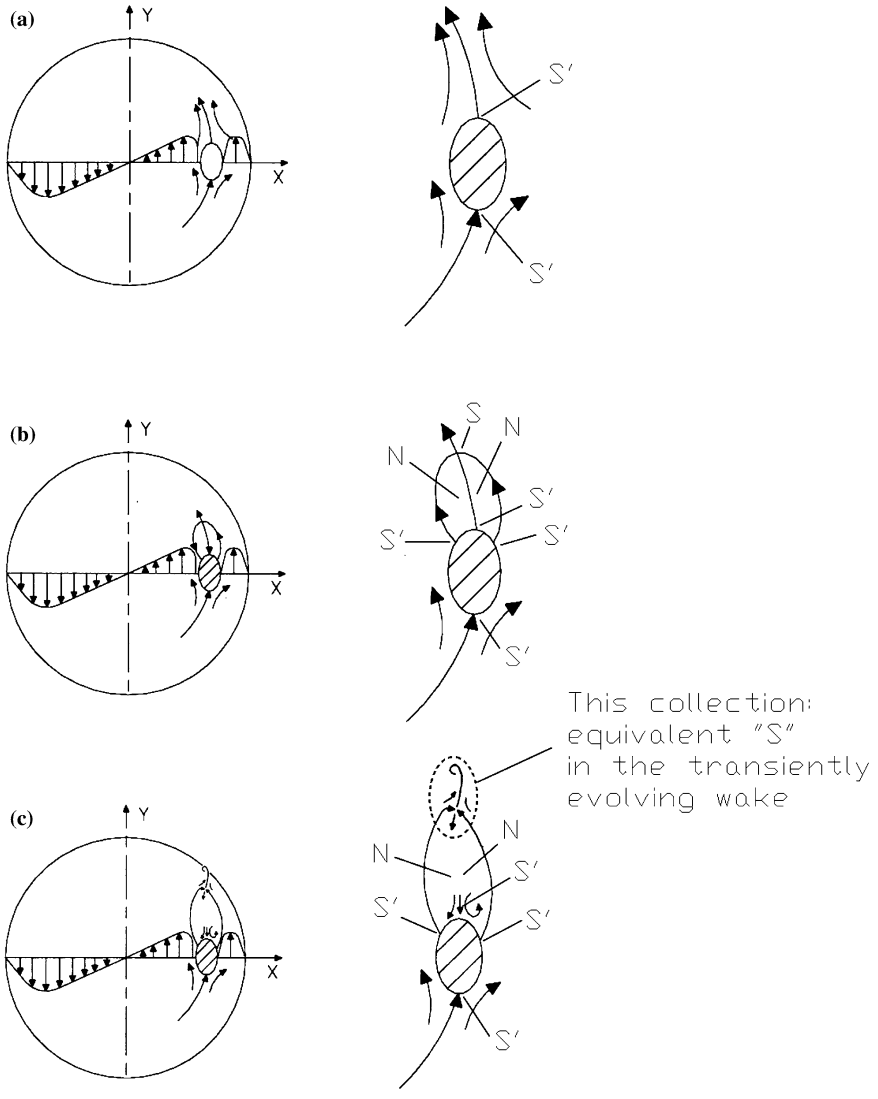

Fig. 9a–c. The stirred cup with the spoon as handle. **a** Low *Re*. **b** Intermediate *Re*. **c** High *Re*

the perimeter of the disc, i.e., the seam, is tangential to the surface, which fulfills the stated constraint. The centered node is the only singular point and it satisfies Eq. 7, since $X_{surface}=2$ for this example. If the stirring spoon were still in the cup, the collapsed surface would be a sphere with a handle. Note that the handle extends across the interior surface of the collapsed sphere. For this case, X=0, which could be satisfied as shown in Fig. 9a, b, c, which schematically exhibit three Reynolds number conditions; low, intermediate, and a high Reynolds number, respectively, developing flow for the flow past the spoon handle.

3.3
Considerations associated with the presence of holes in a selected surface

Figure 10 has been prepared to demonstrate the constraint: either inward or outward pointing vectors at the exposed edge of a hole. Namely, as shown in Fig. 10, the surface of a circular disc can be created by adding one hole to a sphere and then "flattening" the remaining portion of the sphere to a planar disc. (It is important to note that such a disc, $X=1$, is not the same as the "evacuated sphere" at the mid-height of the stirred cup, $X=2$, as considered in

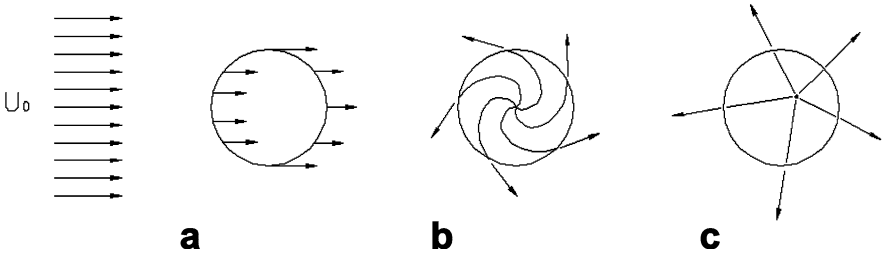

Fig. 10a–c. A disc on the floor of a wind tunnel. **a** Rectilinear flow (U_o). **b** The flow induced by spinning the disc ($U_o=0$). **c** The flow over the disc from an off-center, impinging jet ($U_o=0$)

Fig. 3). For illustration, consider this disc to be placed on the floor of a wind tunnel. It is known a priori that the disc will contain one node on its interior if it satisfies the established constraints of inward or outward directed vectors at its periphery.

Figure 10a shows the consequence of violating the uniform inward—or outward—constraint. The uniform flow of Fig. 10a exhibits no singular point on the disc.

In contrast, and with no tunnel flow, Fig. 10b—a spinning disc—or an axisymmetric jet directed onto the disc as shown in Fig. 10c, satisfy the constraint.

A further example of the "inward/outward vector field at a hole" constraint is provided by a modification to the example of the archer's arrow; see Fig. 6. It is easily recognized that the details of the forward region are independent from the possible complexities of the aft region. It is also apparent that a contour around the central portion of the arrow can be selected such that $\vec{V}$ is outwardly directed at the exposed edge of the forward surface—or inwardly directed for the downstream portion of the arrow. For this condition and for a no-slip or a body fitted surface, the forward and the aft regions are separately characterized as a sphere plus one hole. A zero yaw/pitch condition will clearly lead to one stagnation (i.e., nodal) point at the forward nose. A non-zero yaw or pitch condition will involve an upwind node and some collection of nodes and saddles on the leeward side. If a sock-like surface is placed over the leading section of the arrow, and if its downstream edge satisfies the outward directed velocity condition, then X for this surface is +1. Hence, the leeward side collection of singular points must sum to zero. This latter case has been investigated by numerous authors, given its importance in the aerodynamics of missiles and aircraft (e.g., Tobak and Peake 1979, 1982).

4
An arbitrary constraint and Hunt et al. (1978) revisited

The surface selection process described above has, as a concomitant feature, an alternative description of the surface-mounted obstacles investigated by HAPW (1978). Figures of that reference show the obstacle, and the boundary layer plate to which it is attached, as part of a hypothetical sphere. The corresponding attachment and separation nodes satisfy the X=2 condition for the hypothetical sphere, which results in a net of zero indices for the region of interest. The present alternative is to construct a surface for the evaluation of the region of interest. Consider that a malleable sphere is pressed onto the region of interest such that it conforms to the object and the base plate, and that its top surface exists well above the surface-mounted obstruction. Then, "punch" an upstream and a downstream hole in this sphere; see Fig. 11a. (The relevant surface of the sphere is its interior in this example.) With the sphere's upper, forward, and aft surfaces sufficiently far from the obstruction, it is recognized that the velocity vectors are inward at the upstream hole and outward at the downstream hole. Hence, the region of interest will exhibit no net singular points—in agreement with HAPW (1978)—without invoking a hypothetical body.

It is noteworthy that a detailed study of a surface-mounted cube has been carried out by Martinuzzi and Tropea (1993). The surface streaking images from that study give an insight into the complex flow pattern that must, in the aggregate, yield the same number of nodes as saddles for the body fitted surface.

HAPW (1978) have also provided an example of an obstruction with a passageway that is, in the current context, recognized as a sphere plus two holes plus a handle. The sphere is the same as that described for the surface-mounted obstruction. The obstruction is again attached to the interior surface of the above sphere; see Fig. 11b.

HAPW (1978) further consider the juncture of two pipes and use an image system to deduce the result: $X_{2\text{-pipe juncture}}=-1$. The present technique would address this flow by first distorting a sphere into the shape of the y branch with the two-approach and the one-departure legs of sufficient length such that, when the inlet and exit openings are "punched" through the surface, the velocity is everywhere inward (upstream) and outward (downstream). Given $X_{surface}=X_{sphere}-3$ holes, the result is the same ($X_{surface}=-1$) as that of HAPW without invoking an image system.

For completeness, it is noted that what is referred to here as a collapsed surface was also examined by HAPW (1978) in their study of the flow over a solid obstacle and the one with a passageway. For the present purpose, these would be a sphere plus two holes and a sphere plus two holes and an interior handle, respectively. The collapsed surface is selected such that the velocity vector is aligned with seams as well as meeting the inward/outward constraints. These surfaces can be envisioned by allowing the lateral portions of the Fig. 11a, b surfaces to be collapsed to the centerline of the obstruction.

5
Illustrative examples

The examples in this section are presented to further clarify the above concepts, as well as to provide information about the selected flow fields. These examples, like those of Sect. 3, are for a sphere plus its modifications.

5.1
A levitated sphere

Figure 12 shows a sphere that is levitated and rotated by the action of an inclined jet. The indicated stagnation points of the entrainment flow (see Fig. 12a) can be made evident by dye-in-water or smoke-in-air as the visualization agent. An alternative representation, Fig. 12b, is provided by the centerplane of the jet; this is a sphere with two holes. The lower seam of this collapsed sphere is formed by the lowest time mean streamline from the delivery jet for the surface whose upper boundary is indicated by I. The upper time mean streamline from the top of the jet forms the other seam in the cases shown. A point of interest is that the jet fluid (in its time mean representation) does not touch the sphere. The surface shown by II shares the upper boundary with I; however, its lower surface is a seam that has a centered segment as the seam that touches the lower portion of the levitated sphere. Collapsed surface II is also formed by a sphere with two holes.

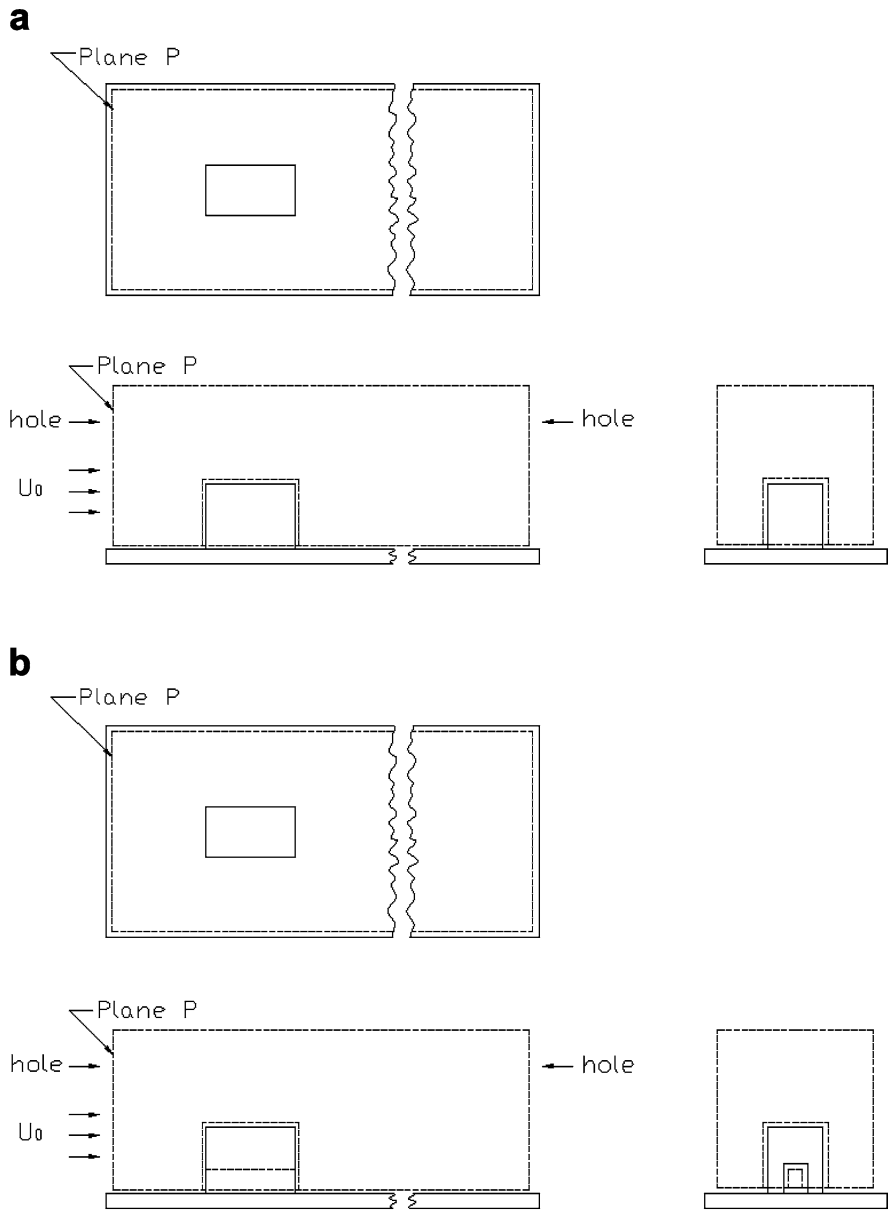

Fig. 11a, b. A surface-mounted obstruction; a representative geometry from Hunt et al. (1978). **a** A solid obstruction; see Martinuzzi and Tropea (1993). **b** An obstruction plus passageway

5.2
Free convection in a Hele-Shaw cell

A second example of a sphere is provided by the free convection flow within a Hele-Shaw cell. The resulting flow field was investigated by Zimmermann et al. (1986). This unpublished study utilized similar experimental techniques as used by Koster and Mueller (1982 and 1984) For convenience, this paper will be referred to as ZEM (1986). Their geometry is shown in Fig. 13a; it is characterized by the relatively large $L\times L$ front and back vertical walls separated by four narrow (width W) walls of area $W\times L$. The magnitudes of these lengths were L=40 mm and W=3 mm (W/L=0.075) in the ZEM (1986) experiment. The interior fluid was heated through the lower surface ($W\times L$) and cooled at the top surface ($W\times L$); $Re=1.5\times10^6$. Interferometric observations reveal a dominant circulation pattern in the upper and central regions, with complementary circulation motions in the lower corner regions, as shown in Fig. 13b.

The ZEM (1986) flow is considered to be an instructive example problem because of the requirement to add additional singular points (beyond those required by the hairy sphere theorem) and because the experimental observations are, at present, not sufficient to clarify the complete flow pattern. That is, the topological inferences, given below, form a prediction that can guide subsequent experimental efforts. If the observed pattern is different from that hypothesized below, it can be usefully checked by ensuring that it satisfies the constraints that are also satisfied by the hypothesized field.

An undeformed sphere ($\mathrm{d}\,A=R^2\mathrm{d}\theta\mathrm{d}\phi$ for $0\le\theta<2\pi$ and $0\le\phi\le\pi$) can be envisioned as a reference case. If the lower region (e.g., $0.9\pi\le\phi\le\pi$ and $0\le\phi<2\pi$) were uniformly heated, whereas a similar cap ($0\le\phi\le0.1\pi$, $0\le\theta<2\pi$) were cooled, then an interior circulation pattern with a vertically rising flow at the center of the sphere would be observed. The lower separation point and the upper attachment point would form the two

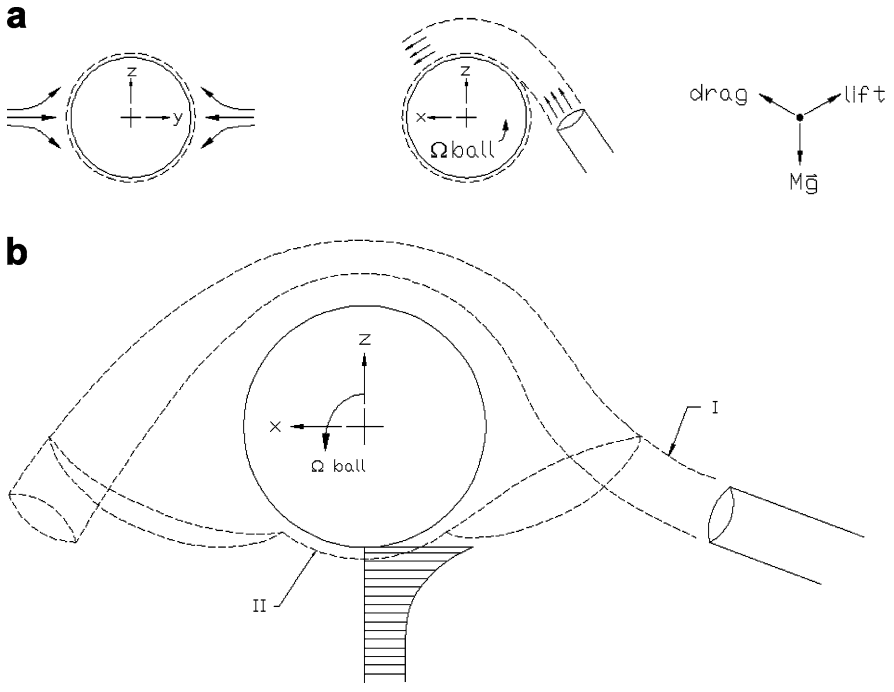

Fig. 12. A levitated sphere

nodes that are required to satisfy the following condition:

$$X_{\text{surface}} = X_{\text{sphere}} = \Sigma N - \Sigma S = 2$$

A collapsed surface, in the form of a circular disc ($0 \le r \le R$, $0 \le \phi < \pi$, and $\theta = \theta_o$, $\theta_o + \pi$), will also have an Euler characteristic of 2; namely:

$$X_{\text{disc}} = 2\Sigma N + \Sigma N' - 2\Sigma S - \Sigma S' = 2$$

(Note that: (1) the velocity field satisfies the condition that the vectors are parallel to the seam for this collapsed surface, and (2) the disc has a small ($<<<R$) but finite thickness, except at the seam.) The two nodes in the collapsed surface for θ_o and $\theta_o + \pi$ and centered at ($\phi = \pi/2$, $r \approx R/2$), and the two 1/2 saddles at $\phi = 0$ and π satisfy the above constraint.

With this background, the large vortex motions, II, III from ZEM (1986), as shown in the present Fig. 13b, are of the kind expected for the above sphere; similarly, these would be consistent with the $\phi = 0$ and π attachment and separation points, respectively. These expected features are shown in the collapsed surface, the $z = 0$ plane, of Fig. 13b as the 1/2 saddles (A, B). This figure also shows two features that are required by the basic flow pattern reported by ZEM (1986), namely, the attachment 1/2 saddles at F_1 and F_2 and the separation points (again, 1/2 saddles) at E_1 and E_2.

The Euler characteristic for the collapsed sphere in the $z = 0$ plane, $X_{\text{surface}} = 2$, is satisfied for this surface as $4N$ and $6S'$, or:

$$2\Sigma N + \Sigma N' - 2\Sigma S - \Sigma S' = 2$$
$$2(4) + 0 - 0 - 6 = 2$$

Additionally, a collapsed sphere in the $y = 0$ plane, see Fig. 13c, satisfies this constraint as:

$$2\Sigma N + \Sigma N' - 2\Sigma S - \Sigma S' = 2$$
$$2(2) + 0 - 0 - 2 = 2$$

Further insight into the flow field of the Hele-Shaw cell can be gained by considering the vorticity filaments associated with the circulations (Γ) of the nodes that are evident in Fig. 13b. The 1/2 planes: *A-D-C-B* and *A-G-E-H-F-B*, will be used for these considerations. (The left-hand side: 1, or the right-hand side: 2, could be used for this discussion. Side 1 will be utilized in the following.) Also, the solenoidal condition, $\nabla \cdot \vec{\omega} = 0$, with its consequence that vorticity filaments (lines in the flow that are everywhere tangential to $\vec{\omega}$), must either form closed loops or terminate at a "physical surface," will be utilized in these considerations.

The contour $\lambda_\alpha = A \to D \to C \to B \to A$ (Fig. 13c) can be used to define Γ_α as:

$$\Gamma_\alpha = \int_B^A u\,dx$$

Using Fig. 13b, a second contour, $\lambda_\beta = A \to G \to E \to F \to B \to A$ and a third contour, $\lambda_\gamma = A \to G \to E \to H \to F \to B \to A$, can be defined with the results:

$$\Gamma_\beta = +\int_B^A u\,dx + \int_{E_k}^{F_k} \vec{V} \cdot d\vec{s}$$

and:

$$\Gamma_\gamma = +\int_B^A u\,dx = \Gamma_\alpha$$

It is evident that $\Gamma_\beta > \Gamma_\alpha$ since the $E \to F$ portion introduces a positive contribution to the circulation.

The "bulk of the vorticity" in region I will exhibit a negative ω_z value given the condition that, for the contour $\lambda_\delta = E \to H \to F \to E$:

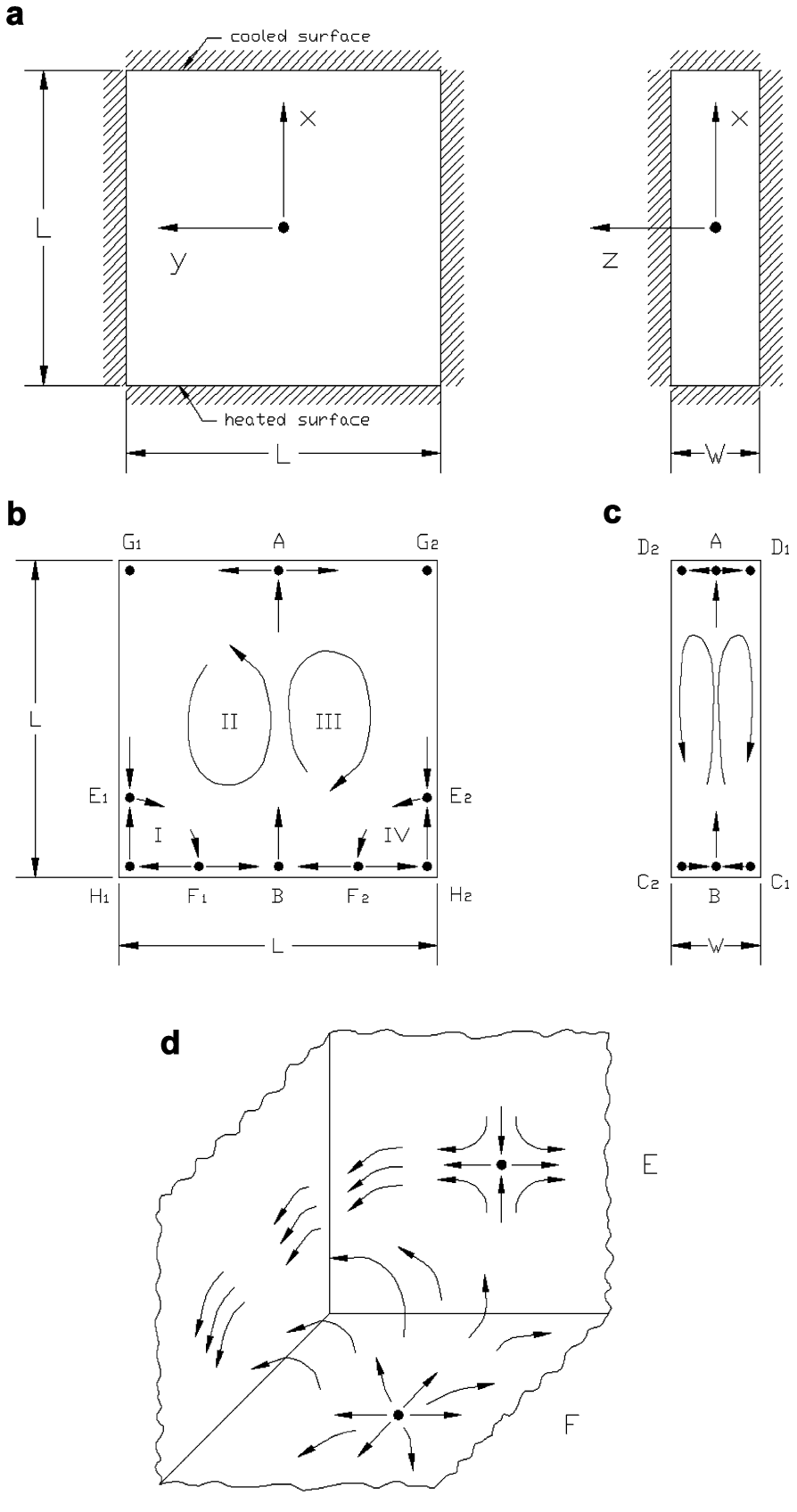

Fig. 13a–d. The free convection experiment of ZEM (1986). **a** The experiment. **b** The observed flow pattern for $Ra=\beta g\Delta t L^3 \nu k$ between 1.27 and 1.95×10^6. **c** Identification of the singular points (*A*, *B*, *E*, *F*) in the $z=0$ and $y=0$ planes. **d** *E* and *F* as a saddle and node, respectively, in the body fitted surface

$$\Gamma_\delta = \int_{\lambda_\delta} \vec{V} \cdot d\vec{s} = \int_{A_\delta} \vec{\omega} \cdot \hat{n} dA < 0$$

This observation, and the constraint, $\Gamma_\beta > \Gamma_\alpha$, leads to the inference that a fraction of the vorticity in II forms closed loops with the vorticity filaments that penetrate I. In effect, sufficient vorticity in II is offset by the vorticity in I that $\Gamma_\gamma = \Gamma_\alpha$. Alternatively, and returning to the original configuration wherein the spherical domain was heated below and cooled above, removing the "cancelled" vorticity in I leaves the balance of the vorticity in II that forms closed loops around the central axis of the Hele-Shaw cell. For completeness, in this description, it is noted that any contour that lies completely at the boundary surface will bound a "net zero" vorticity flux through its enclosed area. Specifically, this observation applies to $A \to D_1 \to C_1 \to B \to C_2 \to D_2 \to A$ and $A \to G_1 \to E_1 \to H_1 \to F_1 \to B \to F_2 \to H_2 \to E_2 \to G_2 \to A$.

With the "picture" in mind of the vorticity filaments that contribute to Γ_α at the $y=0$ plane as those that also penetrate region II above the $E \to F$ contour, it is conjectured that there will be no further singular points of the velocity field beyond those identified above.

The body fitted interior surface of the Hele-Shaw cell is obviously a topological sphere and the attachment node at A and the separation node at B would be sufficient to represent the $X=2$ condition. The above considerations show that singular points E_1, E_2 and F_1, F_2 need to be added to the description as shown in Fig. 13c. Since two saddles (E_1, E_2) and two nodes (F_1, F_2) are added, the Rule is obviously satisfied for this body fitted surface.

5.3
A wind tunnel/centered obstruction flow field

5.3.1
An interpretation of the flow field from the perspective of the rule

The flow field selected by Ruderich and Fernholz (1986) for a detailed examination (hereafter RF) was used (above) as an example of a sphere with three holes (Fig. 8a) and as an example of a sphere with two holes and a handle (Fig. 8b). It is relevant to note that the central thrust of RF was to examine the turbulent boundary layer downstream of reattachment. The present focus, the observed singular points, was a secondary issue in their study.

The body fitted surface (S_0) of Fig. 8a is described by its Euler characteristic as:

$$X_{S_0} = X_{\text{sphere}} - 3 \text{ holes} = 2 - 3 = -1$$

Other, collapsed surfaces will also be of considerable value in the interpretations of the singular points in this flow field. Specifically, consider the collapsed sphere that is positioned at $y=0$, with lateral sides at $z=\pm W/2$, that terminates in a seam at ($x=0$, $y=0$). This surface, S_1, is shown in Fig. 14a. The velocity field at the upstream hole (at $x/W=-10$) satisfies the constraint that it is everywhere inward at the exposed edge. The convention that ()' refers to a half node or a half saddle is not used in Figure 14. The symbols: ()' and ()" are used to specify singular points in the surfaces shown in Figures 14b and 14c respectively.

A second collapsed surface of interest (S_2) is the centerplane ($z=0$) surface with seams along the top of the tunnel, just above the approach centerline, the forward surface of the bluff plate, and the top of the splitter plate, see Fig. 14b. The entrance hole, like that of surface S_1, is located far enough upstream to involve purely streamwise flow; the exit hole is similarly far enough downstream from the time-mean reattachment point on the splitter plate that its farther extension would not involve additional singular points. (The downstream hole is, however, bounded by the top of the channel and the splitter plate).

The topological rules for S_1 and S_2 are also known from their definitions:

$$X_{S_1} = X_{\text{sphere}} - \text{hole} = 2 - 1 = 1$$

and:

$$X_{S_2} = X_{\text{sphere}} - 2 \text{ holes} = 2 - 2 = 0$$

A new experiment, executed in the author's laboratory and described below, has identified six upstream singular points for $z = \pm W/2$, as shown in Fig. 14a. These singular points are similar to those provided by RF (1986). A fourth singular point, the downstream (but $x<0$) N_a of Fig. 6 in RF, was not observed. It is instructive to observe that three half-saddles (−3) and two nodes (+4) contribute a net of +1 on each side of the channel for surface S_1. The required X=+1 for the S_1 surface is then achieved by the contribution of −1 from the centered half-saddle (S'_4). Note that "how to achieve this balance, as well as a smooth vector field," would not be apparent if the fourth side wall singular point of RF were added to Fig. 14a.

The centered plane (i.e., the collapsed sphere of surface S_2) of Fig. 14b is distinctive in that the forward singular point (at $x=y=z=0$) is not on the surface S_2. The seam, that is, everywhere tangential to the velocity, connects to points at $x=-\delta x=-h_P \times 10^{-3}$ "on" the face of the bluff plate. Hence, this seam is above the centered singular point on the face of the bluff plate. The present singular points of Fig. 14b were also identified by RF, except for S'_2 on the downstream surface of the fence. An evaluation of the Rule for Fig. 14b:

$$\underset{(4)}{X = 0} = \underset{(4)}{2\Sigma N} + \underset{(0)}{\Sigma N'} - \underset{(0)}{2\Sigma S} - \underset{(4)}{\Sigma S'},$$

shows that the present collection of singular points meets the required condition. (The RF pattern would not satisfy the Rule for surface S_2.)

Ruderich and Fernholz (1986) provide a photographic record of the surface shear stress pattern on the splitter plate (their Fig. 4a). The singular points along the centerline S'_3 and the inferred N'_1 of Fig. 14b are clearly supported by this image. S'_4 and N'_2 are logically, albeit less obviously, inferred from their Fig. 4a.

Ruderich and Fernholz (1986) prepared a summary representation of the singular points on the splitter plate and the side wall, given the image of their Figs. 4a and 5. This was provided in their Fig. 6. The present author's difficulty in further reconciling the kinematics of the

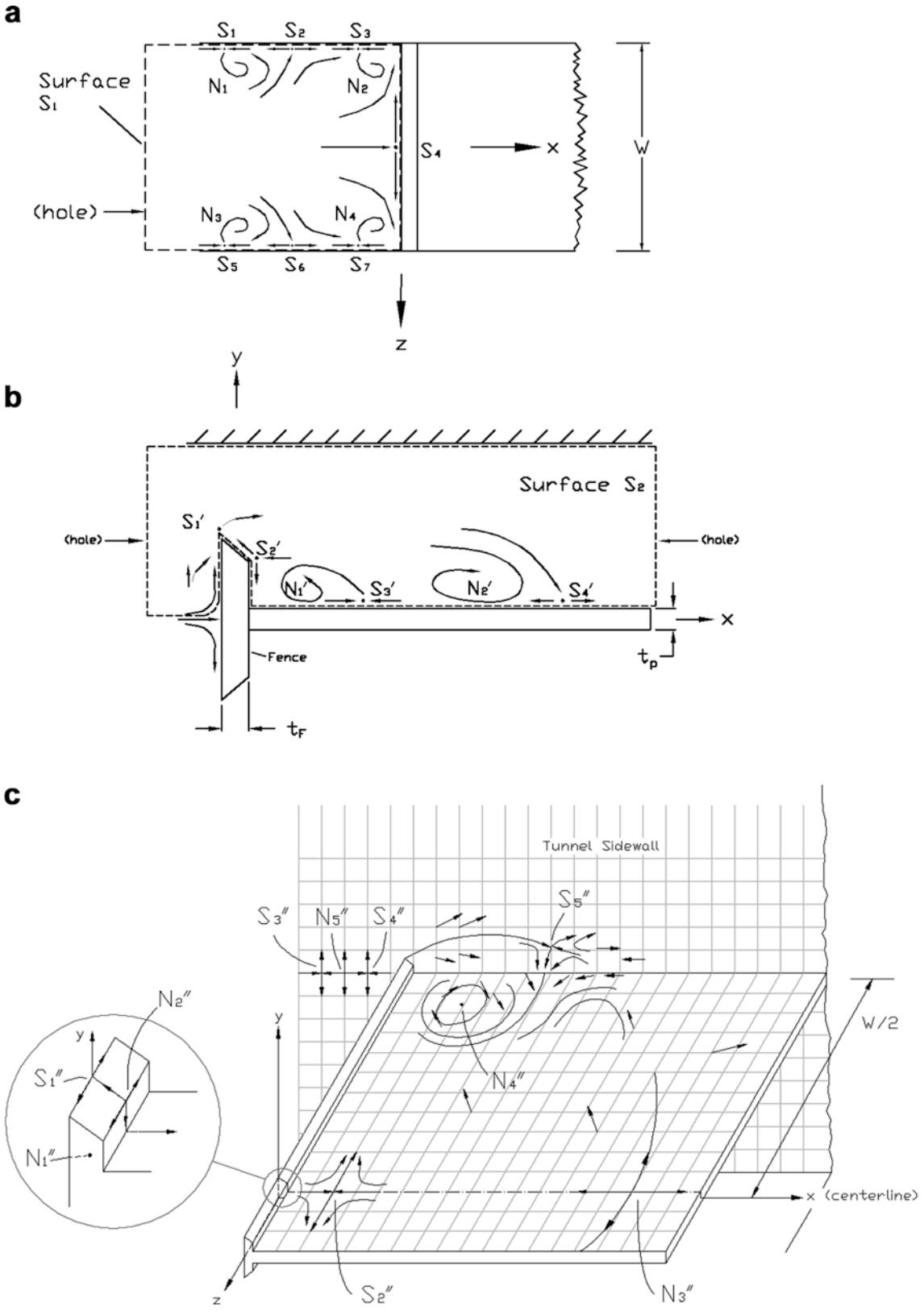

Fig. 14a–c. The experiment of Ruderich and Fernholz (1986). **a** The forward collapsed sphere at y=0, surface S_1 of the RF experiment [$-10h_F<x\le 0$, y=0, $-W/2\le z\le W/2$]. **b** A collapsed sphere bordering the centerline and the tunnel roof, surface S_2 of the RF experiment [$-10h_F<x\le 0$, $y=h_F\times 10^{-3}$, z=0; $\delta n=h_F\times 10^{-3}$ "above" the surface for $h_F\times 10^{-3}\le x\le 17h_F$]. **c** The singular points for the body fitted surface S_0: sphere plus 3 holes as inferred from the new surface streaking observations

Table 2. Identification of the singular points for the geometry of Ruderich and Fernholz (1986) (surface S_0 of Fig. 8)

Domain	N	S
$x<0, y=0, z=\pm W/2$	2 ($N''_5\times 2$)	4 ($2\times S''_3$ and S''_4)
$x=0, y=0$, and $\pm h_F/2$, $z=0$	1 (N''_1)	2 ($S''_1\times 2$)
$x=t_F, y\approx\pm h_F/2$, $z=0$	2 ($N''_2\times 2$)	–
$x>0, y=\pm t_p/2$, $z=0$	2 ($N''_3\times 2$)	2 ($S''_2\times 2$)
$x>0, y=\pm t_p/2$, $\pm z\approx W/2$	4 ($N''_4\times 4$)	–
$x>0$, $\pm y$, $\pm z=\pm W/2$	–	4 ($S''_5\times 4$)
$\Sigma=$	11	12

indicated flow field (Fig. 6 of RF) with both a seemingly logical near wall velocity (i.e., a surface shear stress) pattern as well as the necessary condition provided by the Rule, prompted a recreation of the RF experiment with the same aspect ratio (W/h_F) and Reynolds number based upon h_F. (The blockage in the present study was 6.7% compared with 4.4% for the RF investigation.) Since there are no singular points well above and below the splitter plate, and since the blockage is small in both studies, it is unlikely that this difference between the investigations will play a role in the differences between the reported observations in RF and the present distribution of singular points.

The identified singular points from the new study are shown in Fig. 14c for the surface S_0. (The substantial differences as well as some similarities to Fig. 6 of RF will not be listed since they will be easily recognized from a side-by-side comparison.) The laterally displaced singular points for the $x>0$ region of the S_0 surface were somewhat difficult to discern for the region downstream of the pronounced spiral node and near the corner defined by the side wall and the fence. However, the correct mixture of the carrier liquid (kerosene) and the marking agent provided well defined results.

The "hairs" that would overlay the surface S_o of Fig. 8a would create a smooth vector field and the associated singular points satisfy the Rule; $X_{S_0} = 2 - 3 = -1$. The singular points for this S_0 surface, as identified in the new experiment, are shown in Fig. 14c. For reference, the singular points in each portion of Fig. 14c are tallied in Table 2. The singular point, N''_1 of this S_0 surface is the same singular point as S_4 of the surface S_1, as shown in Fig. 14a.

5.3.2
Commentary on the Ruderich and Fernholz (1986) experimental observations and the current interpretations

The Ruderich and Fernholz (1986) geometry provides a welcome test case for the efficacy of the present method. Specifically:

1. The singular points that have been identified play distinctly different roles depending upon the surface selection. The forward stagnation point, $x=y=z=0$, is a particularly instructive example. It is a node in S_0, it is a half-saddle in S_1, and it was excluded in S_2. If a new collapsed surface were defined that extended S_2 both above and below the splitter plate to create (the new collapsed surface) S_2*, then the $x=y=z=0$ location would have become a half-saddle in a collapsed surface described by a sphere plus three holes.
2. The presence of the singular point on the downstream face of the fence can be argued for by the criterion of a smooth vector field and it is required to satisfy the Rule for S_0 and S_2. It was, however, not identified by RF (1986).
3. If S_0 had been extended past the splitter plate, as shown in Fig. 8b, the geometry would have been changed to a sphere plus two holes and a handle. The Rule would have been changed from $X=-1$ to $x=-2$. This would be satisfied by a "net saddle" at the centerline of the splitter plate's trailing edge.

6
Summary

The basic elements of a *surface selection strategy* and the resulting Rule that identifies the constraints that are placed upon the singular points contained on the selected surface have been presented. These elements, although elementary in the context of topology, are not in widespread use in fluid mechanics publications. The author has, for this reason, attempted to provide an instructive text from which other researchers can adopt and apply these methods for the analysis of their experiments (and possibly of their computations).

These considerations are quite general and they can be applied to any vector field.

Example flow fields are presented and analyzed with these techniques. The significant benefit of using more than one surface to analyze a given flow field is apparent in these examples. A given singular point will represent different characteristics (N, N', S, S') with different surfaces that include that point. The mutual agreement between multiple surfaces will, in general, help to ensure the correct interpretation of the complete flow field.

7
Appendix

The following definition was provided to the author by Professor J.D. McCarthy. It is repeated here for mathematical completeness in relation to the centrally important understanding of a *sphere* in this communication.

An appropriate definition, in the context of the present communication, which is focused on three-dimensional Euclidean space, R^3, can be expressed as follows. A sphere can be understood as that of a smooth two-dimensional submanifold S of R^3 diffeomorphic to the standard two-dimensional sphere S^2 in R^3 (i.e., the set of all points in R^3 at a distance of 1 from the origin (0, 0, 0) of R^3):

1. A subset S of R^3
2. With a smoothly varying two-dimensional tangent space at each point p of S
3. Admitting a smooth map F: $S^2 \rightarrow S$ with a smooth inverse map G: $S \rightarrow S^2$

References

Bredon GE (1993) Topology and geometry. Springer, Berlin Heidelberg New York

Davis HT (1962) Introduction to nonlinear differential and integral equations. Dover, New York, pp 351–355

Hunt JCR, Abell CJ, Peterka JA, Woo H (1978) Kinematical studies of the flows around free or surface-mounted obstacles: applying topology to flow visualization. J Fluid Mech 86:179–200
Hurewicz W (1958) Lectures on ordinary differential equations. Wiley, New York, pp 111–113
Koster JN, Müller U (1982) Free convection invertical gaps. J Fluid Mech 125:429
Koster JN, Müller U (1984) Oscillatory convection in vertical slots. J Fluid Mech 139:363
Lighthill MJ (1963) Attachment and separation in three-dimensional flow. In: Rosenhead L (ed) Laminar boundary layers, vol 2.6. Oxford University Press, Oxford, pp 72–82
Martinuzzi R, Tropea C (1993) The flow around surface-mounted, prismatic obstacles placed in a fully developed channel flow. J Fluid Eng 115(1):85–92
Milnor JW (1997) Topology from the differential viewpoint. Based on notes by Weaver DW. Princeton University Press, New Jersey
Perry AE, Chong MS (1987) A description of eddying motions and flow patterns using critical-point concepts. Annu Rev Fluid Mech 19:125–155
Perry AE, Chong MS (1994) Topology of flow patterns in vortex motions and turbulence. Appl Sci Res 53:357–374
Ruderich R, Fernholz HH (1986) An experimental investigation of a turbulent shear flow with separation, reverse flow, and reattachment. J Fluid Mech 163:283–322
Tobak M, Peake DJ (1979) Topology of two-dimensional and three-dimensional separated flows. In: Proceedings of the AIAA 12th fluid and plasma dynamics conference, Williamsburg, Virginia, July 1979. AIAA paper 79–1480
Tobak M, Peake DJ (1982) Topology of three-dimensional separated flows. Annu Rev Fluid Mech 14:61–85
Zimmermann G, Ehrhard P, Mueller U (1986) Stationäre und Instationäre Konvektion in einer quadratischen Hele-Shaw Zelle, Primärbericht IRB-Nr 507/86 (Mai)